Surface crystallization and magnetic properties of FeCuSiBNbMo melt-spun nanocrystalline alloys

Article *in* Materials Research Bulletin · January 2017

DOI: 10.1016/j.materresbull.2017.01.026

9 authors, including:

Wan Fangpei
Taiyuan University of Technology

Anding Wang
City University of Hong Kong

Chun Tao Chang
Ningbo Institute of Materials Technology and…

G Model
MRB 9119 No. of Pages 6
ARTICLE IN PRESS

Materials Research Bulletin xxx (2016) xxx–xxx

Contents lists available at ScienceDirect

Materials Research Bulletin

journal homepage: www.elsevier.com/locate/matresbu

Surface crystallization and magnetic properties of FeCuSiBNbMo melt-spun nanocrystalline alloys

Fangpei Wan[a,b,c,d], Tao Liu[a,b], Fengyu Kong[e], Anding Wang[a,b,*], Muqin Tian[c,d], Jiancheng Song[c,d], Jianhua Zhang[c,d,**], Chuntao Chang[a,b,*], Xinmin Wang[a,b]

[a] Key Laboratory of Magnetic Materials and Devices, Ningbo Institute of Materials Technology and Engineering, Chinese Academy of Sciences, Ningbo, Zhejiang 315201, China
[b] Zhejiang Province Key Laboratory of Magnetic Materials and Application Technology, Ningbo Institute of Materials Technology and Engineering, Chinese Academy of Sciences, Ningbo 315201, China
[c] College of Electrical and Power Engineering, Shanxi Key Laboratory of Coal Mining Equipment and Safety Control, Taiyuan University of Technology, No. 79 Yingze West Avenue, Wanbolin District, Taiyuan, Shanxi 030024, China
[d] National & Provincial Joint Engineering Laboratory of Mining Intelligent Electrical Apparatus Technology, Taiyuan University of Technology, No. 79 Yingze West Avenue, Wanbolin District, Taiyuan, Shanxi 030024, China
[e] School of Materials and Chemical Engineering, Ningbo University of Technology, Ningbo 315016, China

ARTICLE INFO

Article history:
Received 3 October 2016
Received in revised form 23 December 2016
Accepted 17 January 2017
Available online xxx

Keywords:
A. Fe-based
A. Nanocrystalline alloy
A. Melt-spinning
D. Soft-magnetic property
D. Surface crystallization
D. Thermal stability

ABSTRACT

$Fe_{82}Cu_1Si_4B_{11.5}Nb_{1.5-x}Mo_x$ (x = 0, 0.75 and 1.5 at. %) nanocrystalline alloys were prepared using a melt-spinning technique and the effects of Mo content on thermal stability, soft magnetic properties and microstructure evolution were investigated. It was found that the Mo addition can improve the amorphous-forming ability and inhibit surface crystallization in a low vacuum atmosphere which may be due to better oxidative resistance. All the alloys exhibited excellent soft-magnetic properties with low coercivity of 8.9–10.8 A/m, high effective permeability of 11,500–11,900 at 1 kHz and high saturation magnetic flux density of 1.67–1.72 T after annealing at optimal annealing conditions. In addition, the alloys containing Mo have better transient effective permeability stability with increase in frequency. Decreasing the melt-spinning wheel speed can widen the annealing temperature range for $Fe_{82}Cu_1Si_4B_{11.5}Nb_{1.5}$ ribbon. Results indicate that these soft-magnetic nanocrystalline materials have good manufacturability for industrial production.

1. Introduction

Since the development of $Fe_{73.5}Si_{13.5}B_9Nb_3Cu_1$ (Hitachi ®Finemet) nanocrystalline alloy in 1988 [1], Fe-based nanocrystalline soft-magnetic materials have attracted worldwide attention due to their excellent magnetic properties, including low iron loss due to the low eddy currents in the high frequency range, high effective permeability (μ_e), low saturation magnetostriction (λ_s) and relatively high saturation magnetic flux density (B_s) [2]. They have been widely used in high-frequency transformers, sensors, inductors and many other soft magnetic devices [3]. In order to realize the miniaturization and high efficiency of electrical equipment, improving the flux density, is a major driving force for further alloy compositions development. In the past few years, many high Fe content nanocrystalline alloys such as FeBCu [4], FeSiBCu [5] and FeSiBPCu [6,7] with low iron loss have been developed. These alloys without large radius metallic elements have relatively low glass-forming ability (GFA) and difficult to control annealing processes, which are still big obstacles for mass production [8]. Xiang et al. [9] improved the GFA and enlarged the annealing temperature range of the $Fe_{83}Si_4B_{10}P_2Cu_1$ nanocrystalline alloys by the introduction of niobium (Nb). The addition of refractory metals with large atomic radii such as Mo, Ta, V and Zr, which also suppress grain growth [10–12], was also investigated in other alloy systems. Some issues still remain to be examined, such as the effect of atmosphere and wheel speed in industrial production and development of new alloy systems through

* Corresponding authors at: Key Laboratory of Magnetic Materials and Devices, Ningbo Institute of Materials Technology and Engineering, Chinese Academy of Sciences, Ningbo, Zhejiang 315201, China.
** Corresponding author at: College of Electrical and Power Engineering, Shanxi Key Laboratory of Coal Mining Equipment and Safety Control, Taiyuan University of Technology, No. 79 Yingze West Avenue, Wanbolin District, Taiyuan, Shanxi 030024, China.
E-mail addresses: anding.w@hotmail.com (A. Wang), zhangjianhua@tyut.edu.cn (J. Zhang), ctchang@nimte.ac.cn (C. Chang).

http://dx.doi.org/10.1016/j.materresbull.2017.01.026
0025-5408/

introduction of other elements. These additions should be controlled with regard to the price and the reduction of the B_s. For high B_s alloys with lower content of these elements [13,14] the GFA is close to the glass formation limit for conventional casting technology [15], which maybe result in partial crystallization in the as-cast state, especially at the surface layers. This problem and the unclear effect of a crystallization layer on thermal stability and soft-magnetic properties need to be further investigated.

To elucidate the problems mentioned above, we chose Mo to substitute Nb in FeSiBNbCu alloy for the following reasons: 1) Mo is similar to Nb in physical and chemical properties. It has been proven to inhibit grain growth in Finemet-type alloys [12,16]. 2) It has been reported that the substitution of Nb by Mo in Finemet enhances oxidation resistance [11]. 3) Mo is cheaper and more easily obtainable than Nb, which is particularly appealing for practical use. In this study $Fe_{82}Cu_1Si_4B_{11.5}Nb_{1.5-x}Mo_x$ (x = 0, 0.75 and 1.5 at. %) nanocrystalline soft magnetic alloys with high B_s were prepared in low vacuum atmosphere in the form of melt-spun ribbon and the effects of Mo content on thermal stability, soft magnetic-properties and evolution of the microstructure were explored. The effect of surface crystallization on the soft-magnetic properties of $Fe_{82}Cu_1Si_4B_{11.5}Nb_{1.5}$ ribbons was also investigated. These alloy ribbons exhibited excellent high frequency properties and soft-magnetic properties including high B_s, low H_c and high μ_e after nanocrystallization annealing.

2. Experimental procedure

Multicomponent alloy ingots with nominal compositions $Fe_{82}Cu_1Si_4B_{11.5}Nb_{1.5-x}Mo_x$ (x = 0, 0.75 and 1.5 at. %) were prepared by induction melting mixtures of pure Fe (99.99 wt %), Si (99.999 wt %), B (99.8 wt %), Nb (99.99 wt %), Mo (99.99 wt %), and Cu (99.99 wt %) under a high-purity argon atmosphere. Melt-spun ribbons of these alloys were prepared using the single-roller melt-spinning method and the detail process is given as the following. The master alloys was put into silica crucible after broken into small pieces and the chamber was evacuated to 100 Pa and then filled with argon to 0.02 MPa. Then the master alloys was heated by induction coils and the surface tension of the molten alloy holds the melt inside the crucible until the desired color of the melt is achieved. The melt is then expelled onto the rotating copper wheel with a cooling rate of typically 10^5–10^6 K/s at different wheel speed in argon atmosphere. The prepared ribbons with about 20–40 μm in thickness and approximately 1 mm in width. Thermal properties of the as-spun alloys was evaluated by differential scanning calorimetry (DSC, NETZSCH 404C) at a heating rate of 0.67 °C/s under high argon flow. The as-spun ribbons were cut into 75 mm in length and then subjected to annealing in the absence of magnetic field at various temperatures which were chosen according to the DSC curves for 10 min in a vacuum furnace and subsequently quenched in water with room temperature. The microstructures of the as-spun and annealed ribbons was identified by X-ray diffraction (XRD, Bruker D8 Advance) with Cu-Kα radiation and high-resolution transmission electron microscopy (HRTEM, TECNAIF20). Mean size of the nanocrystalline grains was estimated by using Scherrer equation from the full width at half maximum for the bcc (110) reflection peak and from TEM images. The samples for TEM observation were prepared by ion milling from both sides of the ribbons to examine the structures inside the ribbons. B_s was tested with a vibrating sample magnetometer (VSM) under a maximum applied field of 800 kA/m. H_c were measured by using a DC B–H hysteresis loop tracer under a field of 1000 A/m. μ_e at 1 kHz was measured with a vector impedance analyzer under a field of 1 A/m. All measurements were carried out at room temperature.

3. Results

3.1. Effect of Mo-addition on structure and magnetic properties

The as-spun ribbons prepared by the single-roller melt-spinning method in a low vacuum atmosphere needed for mass production exhibited really good ductility and surface quality. The microstructure of the melt-spun $Fe_{82}Cu_1Si_4B_{11.5}Nb_{1.5-x}Mo_x$ (x = 0, 0.75 and 1.5 at. %) ribbons were characterized by XRD from the free side with different melt-spinning wheel speeds. As shown in the XRD patterns in Fig. 1(a) at Mo content x = 1.5 at. % the ribbon samples were amorphous for all wheel speeds 25 m/s, 35 m/s and 45 m/s. For Mo content x = 0.75 at. % the ribbon samples were crystalline at all wheel speeds. Where Mo content was zero, the

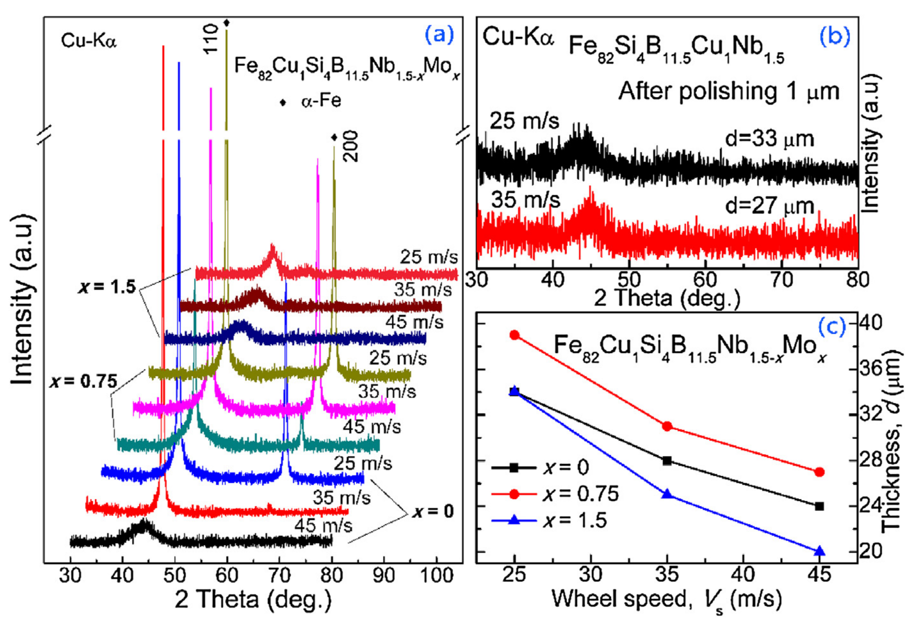

Fig. 1. (a) XRD patterns of the melt-spun $Fe_{82}Cu_1Si_4B_{11.5}Nb_{1.5-x}Mo_x$ (x = 0, 0.75 and 1.5 at. %) ribbons with different wheel speed; (b) XRD patterns of $Fe_{82}Si_4B_{11.5}Cu_1Nb_{1.5}$ ribbons after polishing 1 μm; (c) The thickness of the ribbons with different wheel speed.

sample was amorphous only at the fastest wheel speed 45 m/s and crystalline at 25 m/s and 35 m/s. Moreover, the ribbon is crystalline on the free surface and amorphous where it makes contact with the wheel – as might be expected since the fastest cooling rate will be at the wheel interface. Subsequently, the surface crystallization layers were removed by polishing softly with metallographic abrasive paper and the thickness were measured by spiral micrometer to qualitatively determine the thickness. Fig. 1(b) shows the XRD patterns of $Fe_{82}Si_4B_{11.5}Cu_1Nb_{1.5}$ ribbons after polishing 1 μm and XRD results indicate the thicknesses of the surface crystallization layers are all less than 1 μm. The variation of thickness on the increasing wheel speed was shown in Fig. 1(c). It can be seen that the thickness of the ribbons show a decreases tendency with the increases wheel speed. The ribbons with Nb and Mo co-addition exhibit the highest thickness.

The crystallization process of the melt-spun $Fe_{82}Cu_1Si_4B_{11.5}Nb_{1.5-x}Mo_x$ (x = 0, 0.75 and 1.5 at. %) ribbons were investigated by DSC. As shown in Fig. 2, two obvious exothermic peaks corresponding to two different crystallization phases were detected. According to our previous research, the first exothermic peak corresponds to the crystallization of α-Fe phase and the second corresponds to that of hard magnetic compounds [17,18]. It should be noted that the onset temperature of the first crystallization process T_{x1} decreases slightly, while there is an obvious decreases of onset temperatures for the boride phases precipitation T_{x2} from 585 °C to 568 °C with the increase of Mo content. Consequently, the temperature interval ΔT ($\Delta T = T_{x2} - T_{x1}$) between the two crystal phases decreases from 162 °C to 146 °C [19]. As shown in Fig. 2(b), the exothermic values (ΔH), which corresponding to the area of the first exothermic peak, for the α-Fe precipitation of $Fe_{82}Cu_1Nb_{1.5}Si_4B_{11.5}$ ribbons with 45m/s, 35 m/s and 25 m/s are 119.1 J/g, 115.1 J/g and 114.8 J/g, respectively. After removing the surface crystallization layer of ribbons with 35 m/s and 25 m/s, the exothermic values are 118.8 J/g and 118.5 J/g. The small difference of the exothermic values between polished sample and original sample can indicate the low crystallization fraction.

Changes of H_c for $Fe_{82}Cu_1Si_4B_{11.5}Nb_{1.5-x}Mo_x$ (x = 0, 0.75 and 1.5 at. %) ribbons as a function of annealing temperature (T_A) for 10 min are shown in Fig. 3(a). According to our previous work [20,21], the microstructure evolution during the annealing process of the melt-spun ribbons can be divided into three stages: release of the internal stress, precipitation of α-Fe and precipitation of the hard magnetic phase. Here, we focus on the second and third stages. As shown in Fig. 3(a), all the alloys exhibit a similar tendency. With the increasing of the T_A, the H_c increases at first, and then decreases monotonically between 420 °C and 480 °C, following by another increases. The improvement of the soft-magnetic properties of the samples annealed between T_{x1} and T_{x2} is attributed to the precipitation of α-Fe with fine grain size and high density. While annealed at T_A higher than T_{x2}, the precipitation of the second phase will greatly degrade the soft-magnetic properties. For alloys with x = 0 and 0.75, the optimal T_A is 500 °C, and their lowest H_c is 8.9 A/m and 9.4 A/m, respectively. For the alloy with x = 1.5, the optimal T_A is 480 °C and the corresponding H_c is 10.8 A/m, which is slightly larger than for the other alloys. In addition, the T_A dependence of μ_e of the $Fe_{82}Cu_1Si_4B_{11.5}Nb_{1.5-x}Mo_x$ (x = 0, 0.75 and 1.5 at. %) alloys was also investigated. As shown in Fig. 3(b), the μ_e of all the alloys have a similar tendency in contrast to that of the H_c. With the increase of T_A, μ_e decreases at first and then increases, followed by another decrease. The μ_e for the ribbons with x = 0, 0.75, 1.5 annealed at the optimized annealing temperatures are 11,500, 11,600 and 11,900, respectively. Moreover, it is clear that the Mo bearing alloys exhibit a wider optimal annealing temperature range for low H_c and high μ_e, which is a benefit in mass production.

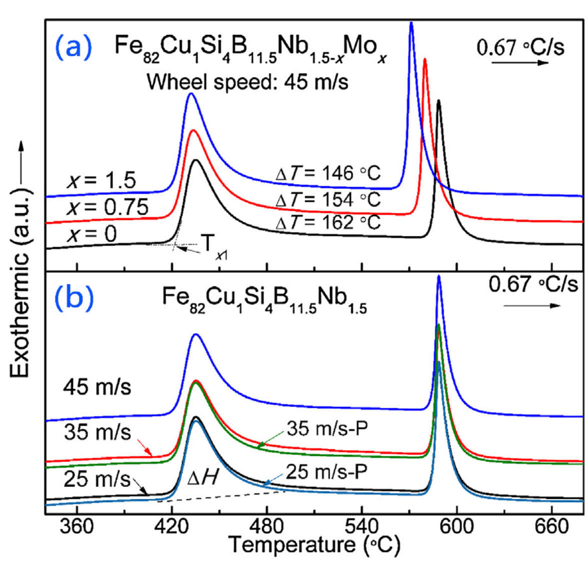

Fig. 2. (a) DSC curves of as-spun $Fe_{82}Cu_1Si_4B_{11.5}Nb_{1.5-x}Mo_x$ (x = 0, 0.75 and 1.5 at. %) ribbons at a heating rate of 0.67 °C/s; (b) The comparison of DSC curves between the unpolished and the polished $Fe_{82}Cu_1Nb_{1.5}Si_4B_{11.5}$ ribbons with different wheel speed.

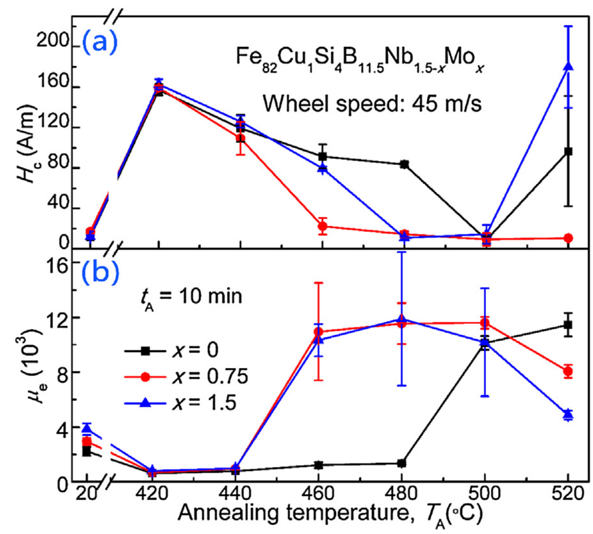

Fig. 3. T_A dependence of H_c (a) and μ_e (b) for the $Fe_{82}Cu_1Si_4B_{11.5}Nb_{1.5-x}Mo_x$ (x = 0, 0.75 and 1.5 at. %) ribbons annealed for 10 min.

The changes of H_c and μ_e as a function of T_A present a tendency of "increase-decrease-increase" or "decrease-increase-increase" which contribute to the evolution of the microstructure [22]. In order to ascertain the microstructure change during the annealing process in the alloys with different Mo content, all samples annealed at respective optimal T_A for 10 min were identified by XRD, as shown in Fig. 4. According to the XRD patterns, the mean grain size (D) which were estimated by the Scherrer equation are 18.8 nm, 19.1 nm and 20.4 nm for x = 0, 0.75 and 1.5 at. %, respectively. Since the atomic radius of Mo (0.136 nm) is smaller than Nb (0.143 nm), its addition is less effective in inhibiting the diffusion of Fe and Si atoms, thus the growth of α-Fe phase occurs more easily. This may be the reason for the grain size increase of $Fe_{82}Cu_1Si_4B_{11.5}Nb_{1.5-x}Mo_x$ alloys with the increase of Mo content.

The B_s of the alloys annealed at optimal annealing condition are shown in Fig. 5. With the substitution of Mo for Nb, B_s shows a monotonic increasing tendency. As shown in Fig. 5(a), B_s of the x = 0, 0.75 and 1.5 samples are 1.67 T, 1.70 T and 1.72 T, respectively,

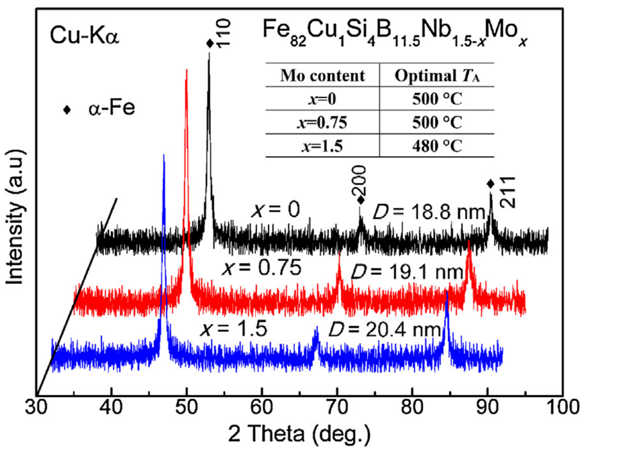

Fig. 4. XRD patterns of $Fe_{82}Cu_1Si_4B_{11.5}Nb_{1.5-x}Mo_x$ (x = 0, 0.75 and 1.5 at. %) alloys ribbons annealed at respective optimal annealing condition.

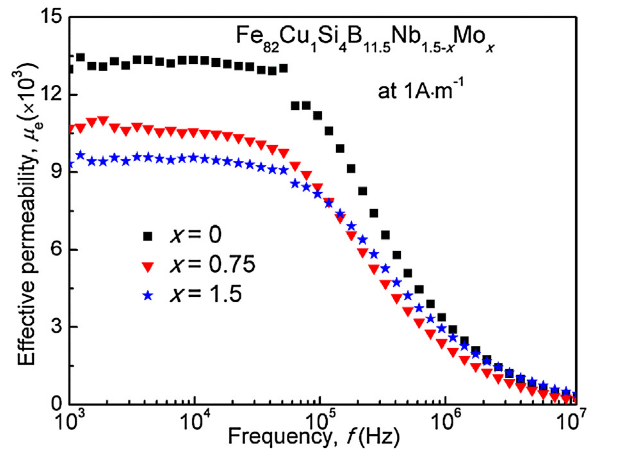

Fig. 6. μ_e as a function of applied field frequency for the $Fe_{82}Cu_1Nb_{1.5-x}Mo_xSi_4B_{11.5}$ nanocrystalline ribbons.

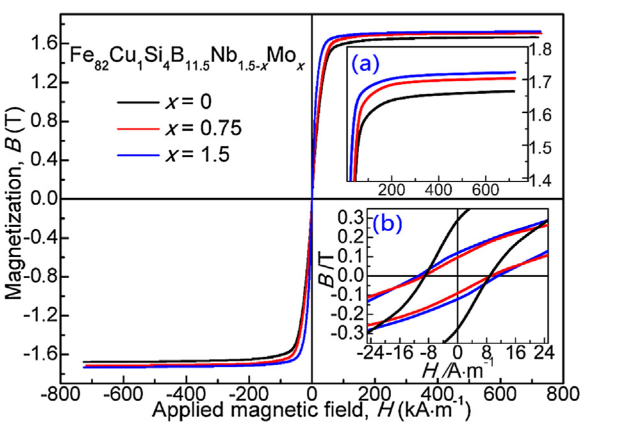

Fig. 5. Magnetic hysteresis loops of $Fe_{82}Cu_1Si_4B_{11.5}Nb_{1.5-x}Mo_x$ (x = 0, 0.75 and 1.5 at. %) alloy ribbons annealed at respective optimized annealing condition. (Inset (a) shows the B_s clearly; inset (b) depicts partially enlarged B-H loop showing the H_c).

while all the samples remain low H_c as we can see in Fig. 5(b). It has been proved [14] that B_s reflects the ratio of the volume fraction of the crystalline phase (V_c/V) to that of the amorphous phase (V_a/V), and can be roughly expressed as $B_s = B_{sc}V_c/V + B_{sa}V_a/V$, where B_{sc} and B_{sa} are the saturation magnetic flux densities of the crystalline and amorphous phases, respectively. Moreover, the B_{sc} is larger than B_{sa} [5]. Since the atomic size of Mo is smaller than Nb, its addition is less effective in inhibiting the diffusion of Fe and Si atoms [12], thus the growth of the Fe(Si) phase is easier, leading to an increase of V_c/V, eventually resulting in increase of B_s. In order to study the effect of Mo on frequency properties, the frequency dependences of μ_e of the annealed $Fe_{82}Cu_1Si_4B_{11.5}Nb_{1.5-x}Mo_x$ (x = 0, 0.75 and 1.5 at. %) alloy ribbons were measured. It can be seen from Fig. 6 that the μ_e is almost constant and independent of frequency in the low-frequency region under a low field for all the samples and then the value of μ_e decreases with an increase of the field frequency. For the Mo-doped alloys, μ_e decreases less rapidly with increasing frequency than Mo-free alloys, that is Mo-doped alloys have good transient μ_e stability with the increasing frequency, which makes these alloys promising for application in high frequency electron devices.

Fig. 7 shows the TEM bright-field image, selected area electron diffraction (SAED) patterns and grain size distributions of $Fe_{82}Cu_1Si_4B_{11.5}Mo_{1.5}$ alloy ribbon annealed at 480 °C for 10 min. The TEM bright-field image in Fig. 7(a) shows that the α-Fe nanocrystals uniformly distributed in the amorphous matrix. The SAED pattern reveals that there are only α-Fe grains without any other compound phases [23]. Since the contrast mainly originated from the diffraction, the different color of the grains in Fig. 7(a) illustrates the random orientation which are good for decreasing the anisotropy. According to the grain size statistics result in Fig. 7(c), the average D of α-Fe grains is about 20.8 nm, which is consistent with the result estimated from XRD (20.4 nm). Since the H_c and μ_e can be roughly interpreted as $H_c \propto D^6$ and $\mu_e \propto D^{-6}$ [9], therefore it is hence concluded that the fine grain size and uniform distribution are the major reason for the good soft magnetic properties.

3.2. Effect of surface crystallization on magnetic properties

In order to elucidate the effect of crystallization layers on magnetic properties of the $Fe_{82}Cu_1Si_4B_{11.5}Nb_{1.5}$ alloy, ribbons were prepared with different quenching rates (wheel speed of 25, 35 and 45 m/s). As shown in Fig. 8, the T_A dependence of H_c and μ_e of the samples with different crystallization surface layers show similar tendency as Fig. 3. It is should be noticed that the samples with surface crystallization layers have a wider annealing temperature range.

As the nucleation of α-Fe is strongly relate to the Cu clusters in FeSiBNbCu system alloys and the primary crystalline is always exist in the as-quenched ribbons with low cooling rate, we suppose that the as-quenched samples with surface crystallization contain a large amount of Cu clusters under the crystallization layers, which serve as nuclei for heterogeneous nucleation of α-Fe crystallites during the annealing process, and α-Fe crystalline phases randomly dispersed on the ribbon surface. When subjected to annealing, large number of α-Fe precipitate and then the grains compete to growth leading to a uniform refine nanocrystalline structure. Therefore the grains need higher annealing temperature with the same annealing time to grow up which will result in large annealing temperature range. It is well known that such a surface crystallization layer results in an out-of-plane magnetic anisotropy and, hence, affect the soft magnetic properties significantly [24,25]. While for some situations, the completely amorphous state is not always advantageous, instead, partial crystallization may lead to improved or even novel properties [24]. It has been reported that iron rich metallic glasses will exhibit excellent high frequency behavior when the amorphous matrix contains very low (0.01–0.05) volume fractions of α-Fe which lead to ferromagnetic domain refinement, result in a reduction in the anomalous eddy current losses [26]. The crystallization volume fractions for

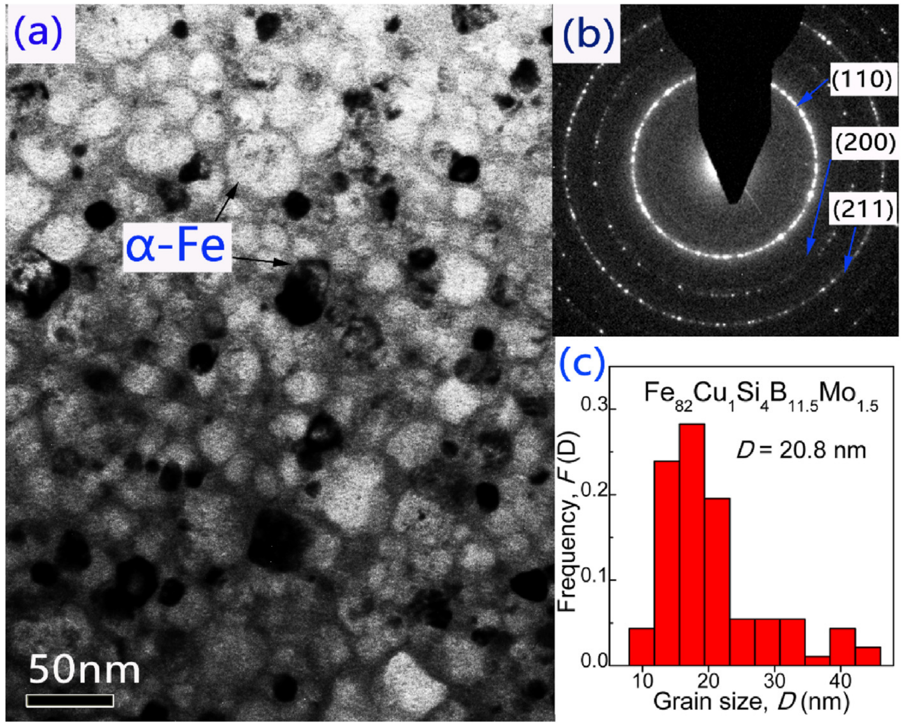

Fig. 7. (a) Microstructure images obtained by TEM with (b) selected area electron diffraction patterns and (c) D distributions for $Fe_{82}Cu_1Si_4B_{11.5}Mo_{1.5}$ alloy ribbon annealed at 480 °C for 10 min.

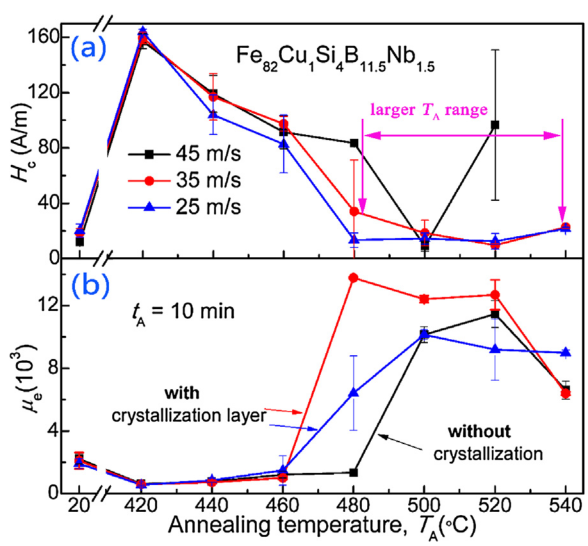

Fig. 8. T_A dependence of (a) H_c and (b) μ_e of $Fe_{82}Cu_1Si_4B_{11.5}Nb_{1.5}$ ribbons with different wheel speed.

$Fe_{82}Cu_1Si_4B_{11.5}Nb_{1.5}$ ribbons with 35 m/s and 25 m/s are less than 0.03, which can be calculated according to the ΔH change of the ribbons with and without polishing in Fig. 2(b).

4. Discussions

Here, we discuss the reason for the effect of the addition of Mo on the GFA and soft-magnetic properties of FeCuSiBNbMo nanocrystalline alloys. According to the atomic size mismatch principle, because the atomic radius of Mo is smaller than Nb this should lead to poor GFA [26]. While the $x = 1.5$ alloy ribbons with completely amorphous microstructure can be easily obtained even with 25 m/s in low vacuum atmosphere. Lopatina et al. [13] have suggested that preferred oxidation at the surface will trigger surface crystallization. Silveyra and Illeková [11] have pointed out that Mo-doped alloys have better oxidative resistance than Nb-doped alloys. Therefore the reasons why the $x = 1.5$ alloy have better GFA can be explained by better oxidative resistance in low vacuum atmosphere. In addition, the estimated B_{sa} is higher in alloys with more Mo than in standard composition Finemet [27]. The high B_s of Mo containing alloys can be explained by the increased crystallization volume fraction (which can be drawn from XRD in Fig. 4) and the higher B_{sa}.

Mo affects the formation and growth of α-Fe is similar to that of Nb in the FeSiBNbCu alloy systems [1]. Because the solubility of Mo in α-Fe is very limited, Mo atoms are rejected from α-Fe nanocrystals and enriched in the remaining amorphous phase. The diffusion of Fe via Mo-rich region (i.e. remaining amorphous matrix) is difficult and such area can act as an obstacle against Fe diffusion because of the large atomic radius of Mo. Hence, the fast growth of nanocrystal is suppressed during the annealing process, resulting in a small grain size. The effect of these refractory elements with large atomic radius has been confirmed [28,29]. But Mo is not as effective as Nb in α-Fe grain growth suppression [16] which leads to a larger α-Fe grains with average D about 21 nm compared to alloys containing Nb with average D about 16 nm. During this growth suppression, more bcc-Fe grains with relatively small D were formed resulting in excellent soft-magnetic properties in the nanocrystalline alloys.

5. Conclusions

In this work the effects of Mo on the soft-magnetic properties, crystallization behavior and the evolution of microstructure of $Fe_{82}Cu_1Si_4B_{11.5}Nb_{1.5-x}Mo_x$ ($x = 0$, 0.75 and 1.5 at. %) nanocrystalline alloys were investigated. We found that adjusting the Mo content improves the formation of an amorphous phase in $Fe_{82}Cu_1Si_4B_{11.5}Nb_{1.5-x}Mo_x$ alloys. When subjected to annealing under optimal condition, all alloys show excellent soft-magnetic properties including low H_c of 8.9–10.8 A/m, high μ_e of 11,500–11,900 and high B_s of 1.67–1.72 T. The Mo-doped alloys have better transient μ_e stability with increase in frequency than the Mo-free alloy, which make these soft-magnetic nanocrystalline alloys suitable for industrial production.

Acknowledgements

This work was supported by the National Natural Science Foundation of China (Grant Nos. 51541106, U1210112 and 51577123), Ningbo International Cooperation Projects (Grant No. 2015D10022), Ningbo Major Project for Science and Technology (Grant No. 2014B11012) and the Qualified Personnel Foundation of Taiyuan University of Technology (QPFT) (No: tyutrc-201370a).

References

[1] Y. Yoshizawa, S. Oguma, K. Yamauchi, New Fe-based soft magnetic alloys composed of ultrafine grain structure, J. Appl. Phys. 64 (1988) 6044.
[2] G. Herzer, Soft-magnetic nanocrystalline materials, Scr. Metall. Mate. 33 (1995) 1741–1756.
[3] M.E. McHenry, D.E. Laughlin, Nano-scale materials development for future magnetic applications, Acta Mater. 48 (2000) 223–238.
[4] M. Ohta, Y. Yoshizawa, New high-Bs Fe-based nanocrystalline soft magnetic alloys, Jpn. J. Appl. Phys. 46 (2007) L477–L479.
[5] M. Ohta, Y. Yoshizawa, Cu addition effect on soft magnetic properties in Fe–Si–B alloy system, J. Appl. Phys. 103 (2008) 07E722.
[6] A.D. Wang, H. Men, B.L. Shen, G.Q. Xie, A. Makino, A. Inoue, Effect of P on crystallization behavior and soft-magnetic properties of $Fe_{83.3}Si_4Cu_{0.7}B_{12-x}P_x$ nanocrystalline soft-magnetic alloys, Thin Solid Films 519 (2011) 8283–8286.
[7] H.M.A. Makino, T. Kubota, K. Yubuta, A. Inoue, New Fe-metalloids based nanocrystalline alloys with high B_s of 1.9T and excellent magnetic softness, J. Appl. Phys. 105 (2009) 07A308.
[8] M.O.Y. Yoshizawa, Effect of heating rate on soft magnetic properties in nanocrystalline $Fe_{80.5}Cu_{1.5}Si_4B_{14}$ and $Fe_{82}Cu_1Nb_1Si_4B_{12}$ alloys, Appl. Phys. Express 2 (2009) 023005.
[9] Z. Xiang, A. Wang, C. Zhao, H. Men, X. Wang, C. Chang, D. Pan, Optimization of thermal stability and soft-magnetic properties of FeSiBPCuNb alloys by Nb content tuning, J. Alloys Compd. 622 (2015) 1000–1004.
[10] J.M. Borrego, C.F. Conde, A. Conde, Structural relaxation processes in FeSiB-Cu (Nb, X), X = Mo, V, Zr, Nb glassy alloys, Mater. Sci. Eng. A 304–306 (2001) 491–494.
[11] J.M. Silveyra, E. Illeková, Effects of air annealing on Fe–Si–B–M–Cu (M = Nb, Mo) alloys, J. Alloys Compd. 610 (2014) 180–183.
[12] Y. Yoshizawa, K. Yamauchi, Magnetic properties of Fe–Cu–M–Si–B (M = Cr, V, Mo, Nb, Ta, W) alloys, Mater. Sci. Eng. A 133 (1991) 176–179.
[13] E. Lopatina, I. Soldatov, V. Budinsky, M. Marsilius, L. Schultz, G. Herzer, R. Schäfer, Surface crystallization and magnetic properties of $Fe_{84.3}Cu_{0.7}Si_4B_8P_3$ soft magnetic ribbons, Acta Mater. 96 (2015) 10–17.
[14] M. Ohta, Y. Yoshizawa, High Bs nanocrystalline $Fe_{84\text{-}x\text{-}y}Cu_xNb_ySi_4B_{12}$ alloys (x = 0.0–1.4, y = 0.0–2.5), J. Magn. Magn. Mater. 321 (2009) 2220–2224.
[15] A. Makino, H. Men, K. Yubuta, T. Kubota, Soft magnetic FeSiBPCu heteroamorphous alloys with high Fe content, J. Appl. Phys. 105 (2009) 4.
[16] W. Lu, J. Fan, Y. Wang, B. Yan, Microstructure and magnetic properties of $Fe_{72.5}Cu_1M_2V_2Si_{13.5}B_9$ (M = Nb Mo, (NbMo), (MoW)) nanocrystalline alloys, J. Magn. Magn. Mater. 322 (2010) 2935–2937.
[17] A.D. Wang, H. Men, C.L. Zhao, C.T. Chang, R.W. Li, X.M. Wang, Crystallization behavior of FeSiBPCu nanocrystalline soft-magnetic alloys with high Fe content, Sci. Adv. Mater. 7 (2015) 2721–2725.
[18] N. Mattern, A. Danzig, M. Miiller, Effect of Cu and Nb on crystallization and magnetic properties of amorphous $Fe_{77.5}Si_{15.5}B_7$ alloys, Mater. Sci. Eng. A 194 (1995) 77–85.
[19] J.M. Silveyra, E. Illeková, P. Švec, D. Janičkovič, A. Rosales-Rivera, V.J. Cremaschi, Phase transformations in Mo-doped FINEMETs, Physica B 405 (2010) 2720–2725.
[20] Z. Li, A. Wang, C. Chang, Y. Wang, B. Dong, S. Zhou, Synthesis of FeSiBPNbCu nanocrystalline soft-magnetic alloys with high saturation magnetization, J. Alloys Compd. 611 (2014) 197–201.
[21] Y. Han, A. Wang, A. He, C. Chang, F. Li, X. Wang, Improvement of magnetic properties, microstructure and magnetic structure of Fe73.5Cu1Nb3Si15.5B7 nanocrystalline alloys by two-step annealing process, J. Mater. Sci.: Mater. Electron. 27 (2015) 3736–3741.
[22] G. Herzer, Grain size dependence of coercivity and permeability in nanocrystalline ferromagnets, IEEE Trans. Magn. 26 (1990) 1397–1402.
[23] J. Torrens-Serra, I. Peral, J. Rodriguez-Viejo, M.T. Clavaguera-Mora, Microstructure evolution and grain size distribution in nanocrystalline FeNbBCu from synchrotron XRD and TEM analysis, J. Non-Cryst. Solids 358 (2012) 107–113.
[24] G. Herzer, H.R. Hilzinger, Surface crystallisation and magnetic properties in amorphous iron rich alloys, J. Magn. Magn. Mater. 62 (1986) 143–151.
[25] H.N. Ok, A.H. Morrish, Origin of the perpendicular anisotropy in amorphous $Fe_{82}B_{12}Si_6$ ribbons, Phys. Rev. B 23 (1981) 2257–2261.
[26] A. Inoue, Stabilization of metallic supercooled liquid and bulk amorphous alloys, Acta Mater. 48 (2000) 279–306.
[27] J.M. Silveyra, V.J. Cremaschi, D. Janičkovič, P. Švec, B. Arcondo, Structural and magnetic study of Mo-doped FINEMET, J. Magn. Magn. Mater. 323 (2011) 290–296.
[28] K. Hono, K. Hiraga, Q. Wang, A. Inoue, T. Sakurai, The microstructure evolution of a $Fe_{73.5}Si_{13.5}B_9Nb_3Cu_1$ nanocrystalline soft magnetic material, Acta Metall. Mater. 40 (1992).
[29] K. Suzuki, J.M. Cadogan, V. Sahajwalla, A. Inoue, T. Masumoto, The role of alloying elements in Cu-free nanocrystalline Fe-Nb-B soft magnetic alloys, Mater. Sci. Eng. A 226–228 (1997) 554–558.

Please cite this article in press as: F. Wan, et al., Surface crystallization and magnetic properties of FeCuSiBNbMo melt-spun nanocrystalline alloys, Mater. Res. Bull. (2017), http://dx.doi.org/10.1016/j.materresbull.2017.01.026